MEMS Deformable Mirrors for Adaptive Optics in Astronomical Imaging

Steven A. Cornelissen
Boston Micromachines Corporation,
108 Water St, Watertown, MA 02472

Paul A. Bierden
Boston Micromachines Corporation,
108 Water St, Watertown, MA 02472

Thomas G. Bifano
Boston University, Dept. Manufacturing Engineering
15 St. Mary's St., Brookline, MA 02446

Jason B. Stewart
Boston University, Dept. of Electrical Engineering
8 St. Mary's St., Boston MA 02048

ABSTRACT

We report on the development of micro-electromechanical (MEMS) deformable mirrors designed for ground and space-based astronomical instruments intended for imaging extra-solar planets. Three different deformable mirror designs, a 1024 element continuous membrane (32x32), a 4096 element continuous membrane (64x64), and a 331 hexagonal segmented tip-tilt-piston are being produced for the Planet Imaging Concept Testbed Using a Rocket Experiment (PICTURE) program, the Gemini Planet Imaging Instrument, and the visible nulling coronograph developed at JPL for NASA's TPF mission, respectively. The design of these polysilicon, surface-micromachined MEMS deformable mirrors builds on technology that was pioneered at Boston University and has been used extensively to correct for ocular aberrations in retinal imaging systems and for compensation of atmospheric turbulence in free-space laser communication. These light-weight, low power deformable mirrors will have an active aperture of up to 25.2mm consisting of thin silicon membrane mirror supported by an array of 1024 to 4096 electrostatic actuators exhibiting no hysteresis and sub-nanometer repeatability. The continuous membrane deformable mirrors, coated with a highly reflective metal film, will be capable of up to 4μm of stroke, have a surface finish of <10nm RMS with a fill factor of 99.8%. The segmented device will have a range of motion of 1um of piston and a 600 arc-seconds of tip/tilt simultaneously and a surface finish of 1nm RMS. The individual mirror elements in this unique device, are designed such that they will maintain their flatness throughout the range of travel. New design features and fabrication processes are combined with a proven device architecture to achieve the desired performance and high reliability. Presented in this paper are device characteristic and performance results of these devices.

1. INTRODUCTION

Adaptive optics are used extensively in the field of astronomy in the pursuit of achieving diffraction limited performance of the optical systems [1]. Deformable mirror technology is key to these adaptive optics systems, correcting for aberrations induced by the atmosphere and imperfections in the fixed optics used in these instruments. Microelectromechanical systems (MEMS) are the foundation of a new class of deformable mirrors, batch fabricated using polysilicon surface-micromachining techniques, providing compact devices, scalable to thousands of actuators, capable of correcting high order aberrations with high precision and repeatability. Segmented MEMS mirrors and continuous face sheet MEMS mirrors are available commercially with up to 1024 actuators. Such mirrors have proven the ability to create reliable micromirror arrays capable of micrometers of deflection in an all-silicon, space-compatible structure. Continuous facesheet devices with 4096 elements and an actuator throw of more than 4μm are in development for the Gemini Planet Imager seeking to find extrasolar Jovian planets from an earth-based observatory [2]. For space-based planet finding applications, a 1024 element continuous facesheet MEMS DM will be used in a mission to image an extrasolar giant planet for the first time. A new MEMS DM is also being developed

for NASA's Terrestrial Planet Finding mission (TPF) [3], which seeks to image extrasolar earth-like planets, having a 331 array of hexagonal elements in which each segment must be flat to within a few nanometers (RMS), and it must remain comparably flat as it is moved in piston or tilt modes.

2. CONTINUOUS FACESHEET MEMS DMs

Boston Micromachines' MEMS deformable mirrors are based on the surface-micromachined, poly-silicon double cantilever actuator architecture pioneered at Boston University [4,5], illustrated in figure 1. The device structure consists of actuator electrodes underneath a double cantilever flexure, the actuator, which is electrically isolated from the electrodes and maintained at a ground potential. The actuators are arranged in a square grid, on a pitch of 300-400μm, and the flexible mirror surface is connected to the center of each actuator through a small attachment post that translated the actuator motion to a mirror surface deformation.

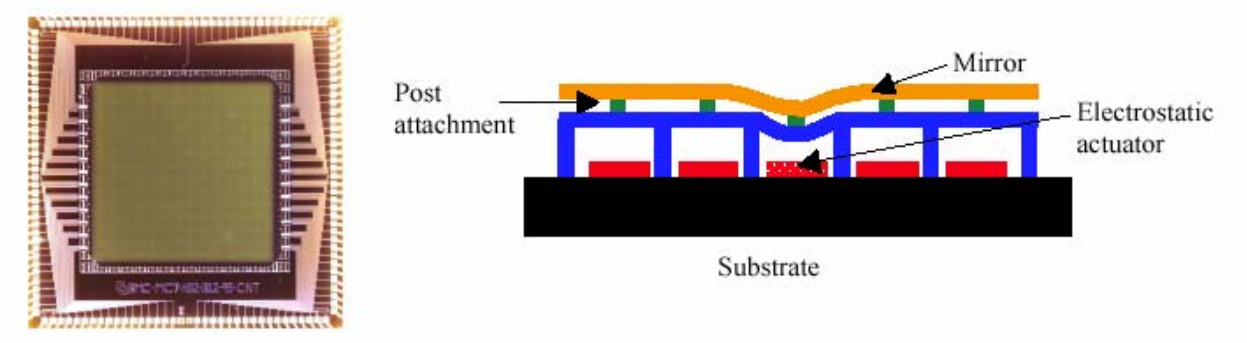

Figure 1. Cross-section of 1x3 electro-statically actuated MEMS deformable mirror.

This MEMS DM architecture allows for local deformation of the mirror membrane with an influence function between 20-40% on its nearest neighbor, depending on the specific device design (see figure 2**)**.

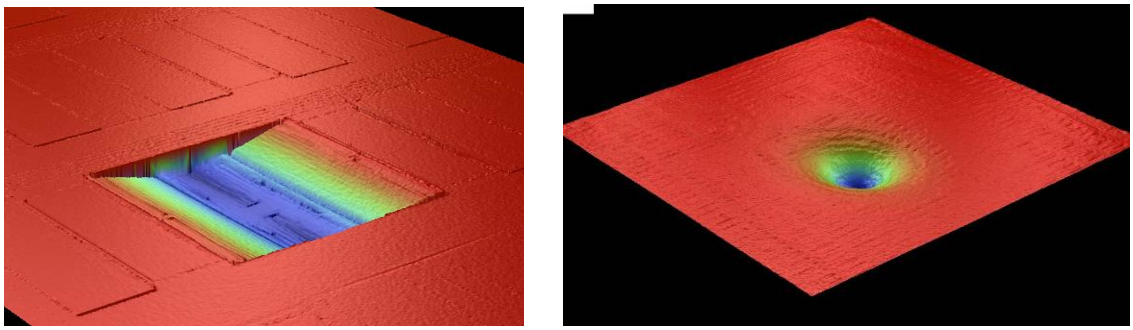

Figure 2. Surface measurement of a single deflected actuator of a 144 element DM (left) and the resulting mirror surface figure of the MEMS continuous face sheet.. The influence of the single element (~35% on device shown) deflection only affects its immediate neighbors leaving the rest of the mirror surface unchanged.

This allows the DM to correct for high order aberrations in the optical path. Shown in figure 3 are wavefront measurements that were generated using a 140 element, 2.5μm stroke, BMC MEMS DM in a closed-loop system, demonstrating the ability of the DM to take the shape of high-order Zernike terms – up to 7th order (35th term).

Electrostatics is used to achieve mirror deformation at each actuation point using an actuator illustrated in figure 4. The actuator has an initial gap, $\boldsymbol{g}$, between the flexure and the fixed electrode. An applied potential, $\boldsymbol{V}$, results in an attractive electrostatic force that bends the actuator membrane downward. As the flexure bends, an elastic (mechanical) restoring force acts in the opposite direction. At equilibrium these two forces balance and the equilibrium deflection at the membrane mid-span is $\boldsymbol{z}$. The equilibrium deflection is a nonlinear increasing function of $\boldsymbol{V}$. Until the voltage is raised to a point where the equilibrium deflection is equal to a little more than one third of the initial gap, the equilibrium is stable. Above that voltage, electrostatic forces are so large that they cannot be balanced by mechanical restoring forces, and the actuator membrane crashes unstably into the fixed electrode. In practice, this unstable region is generally avoided. Fundamentally a parallel plate electrostatically driven actuator can only travel one-third of the gap between the flexure and the electrode before the instability is reached.

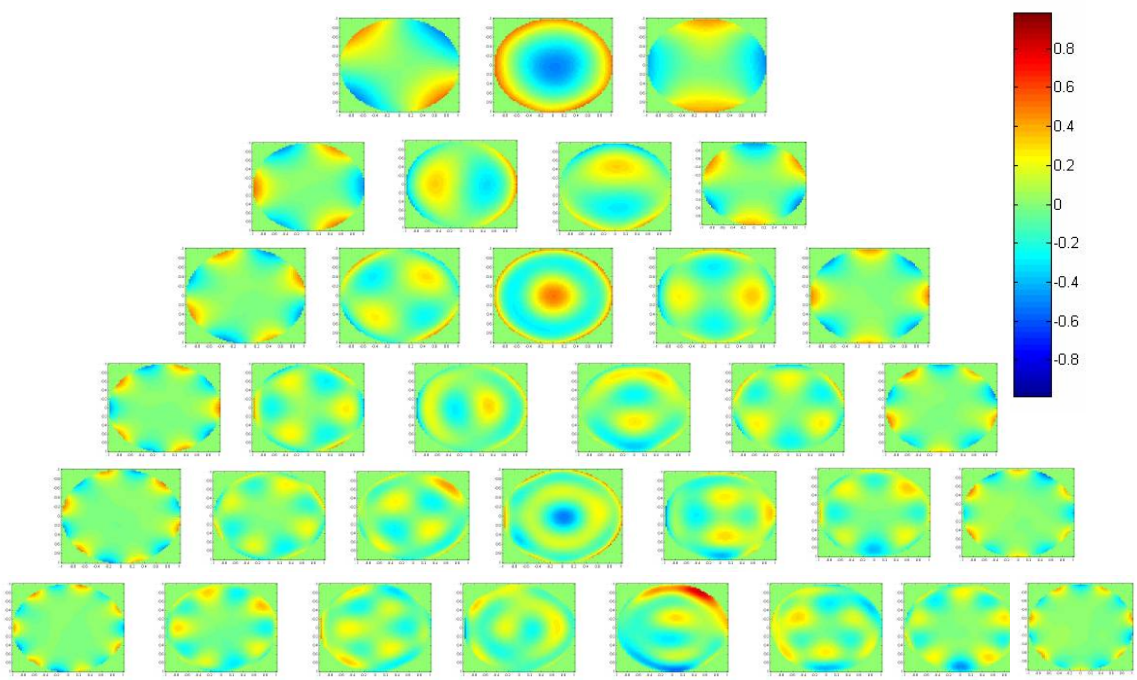

Figure 3. Zernike shapes made by a 2.5µm stroke BMC DM, from 2nd to 7th order (orders by row).Measurements made using a Shack-Hartmann wavefront sensor in a closed-loop control system.

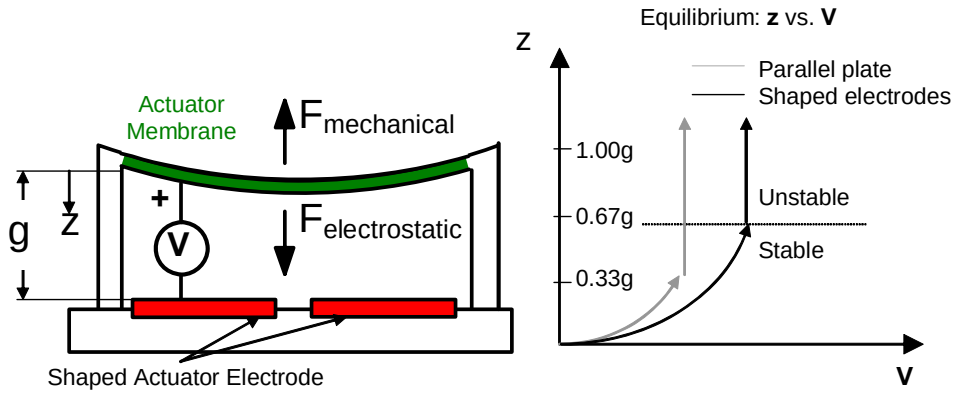

Figure 4. Schematic of electrostatic actuation of a double cantilever actuator used in the MEMS deformable mirror design. The MEMS DM consists of a 2-D array of these actuators each supporting a post attached to the back of the flexible mirror facesheet (not shown in illustration).

A shaped electrode design may be used to achieve higher actuator throw by eliminating the electrostatic attractive force beneath the area of the actuator membrane in which the separation between the flexure and electrode are smallest due to plate bending effects. The cost of using shaped electrodes to achieve longer stroke is higher actuation voltages for a given actuator geometry. To reduce the maximum operating voltage of the DM to the desirable level, the mechanical stiffness of the actuator is modified. These polysilicon electrostatic actuators, used to create deformation in the continuous facesheet or mirror segments of the MEMS DMs presented here, are not significantly affected by operating temperatures (figure 5), do not suffer from fatigue due to cycling (figure 6), and provide hysteresis free operation (figure 7).

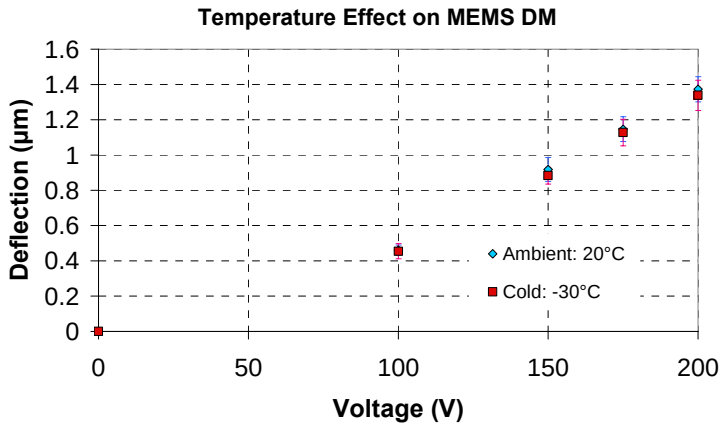

Figure 5. Comparison of the voltage vs. deflection behavior of a MEMS DM at 20ºC and -30ºC. No change in this characteristic is measured.

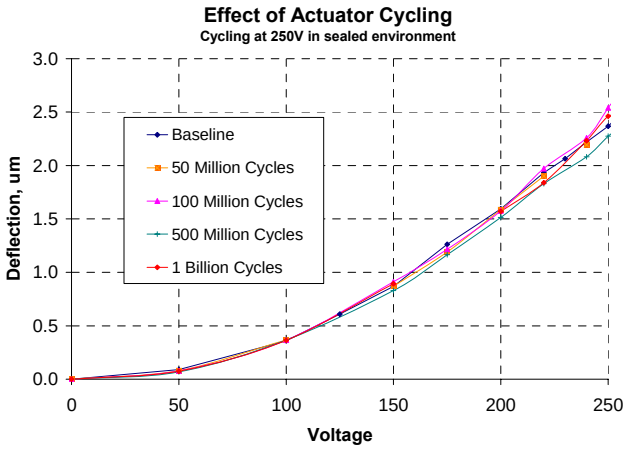

Figure 6. Electromechanical behavior of MEMS DM showing no degradation in performance after cycling the device 1 billion times from 0-250V.

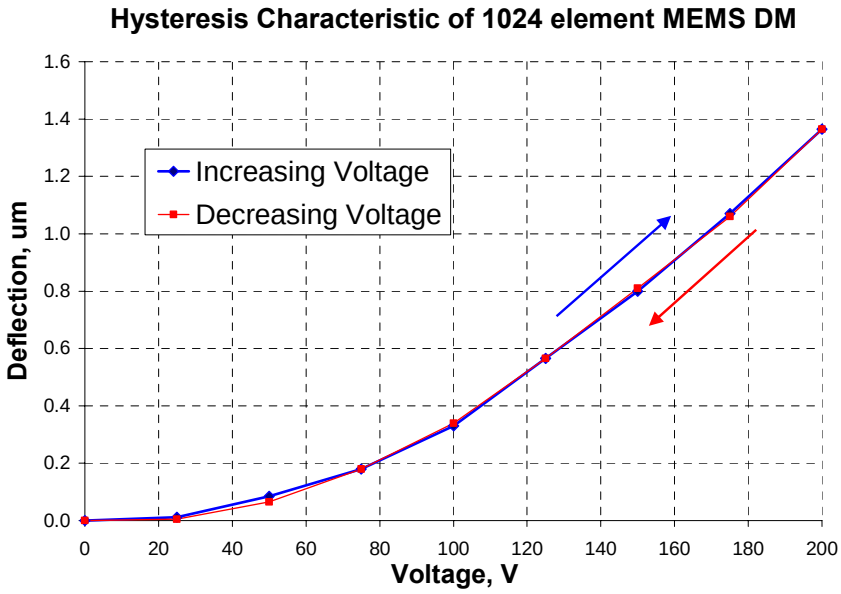

Figure 7. Deflection data of a 1024 element continuous facesheet MEMS DM showing that the electrostatic actuator does not exhibit hysteresis effects (Blue line: increasing voltage, Red line: decreasing voltage)

3. 1024 ELEMENT CONTINUOUS FACESHEET MEMS DM FOR PLANET IMAGING CONCEPT TESTBED USING A ROCKET EXPERIMENT (PICTURE)

The objective of the Planet Imaging Concept Testbed using a Rocket Experiment (PICTURE) program is to make the first direct image of an extrasolar giant planet. This space-based astronomical observation platform will use a visible nulling-interferometer to achieve a contrast ratio of 10^6, in the 500-800nm wavelength regime, such that the starlight is sufficiently suppressed to provide a direct image of the planet epsilon Eri. To achieve this high contrast ratio a 1024 element MEMS DM will be used in the interferometer to correct for any residual wavefront error caused by imperfections in the optical system. By compensating for these errors by adjusting fractions of the pupil at the Angstrom level a Strehl ratio of 0.999999 can be achieved. The performance specifications for the 1024 MEMS DM that will be used for this program, shown in figure 8**,** are listed in Table 1.

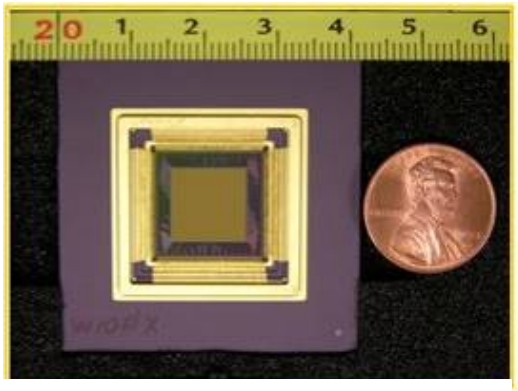

Figure 8. Boston Micromachines Corp. 1024 element MEMS DM

Table 1: BMC µDM1024 Performance Specifications

Number of actuators	1024 (32x32 array)
Actuator pitch	340µm
Fill factor	99.5%
Actuator stroke	2µm (3x3 @220V)
Flatness (unactuated)	16nm RMS
Bandwidth (vacuum/air)	60kHz /7kHz
Aperture	10.2mm

This device was demonstrated to be capable of flattening a wavefront 0.54nm RMS within the active control band (12.8nm RMS total), in a high-contrast imaging testbed using a 13-bit, closed-loop control system [6]**.** Figure 9, shows these results, measured with a phase shifting diffraction interferometer. The initial wavefront, with no active control is measured to be 148nm RMS which is reduced to 12.8nm RMS using the active DM control. The periodic pattern apparent in the wavefront measurement is due to small periodic imperfections on the surface of the continuous mirror facesheet, at the same pitch of the actuator array, resulting from the MEMS fabrication processes. By applying a high-spatial frequency filter to remove these wavefront effects which are outside the region of controllable errors, the flattened wavefront inside the range of controllable errors is measured to be 0.54nm RMS.

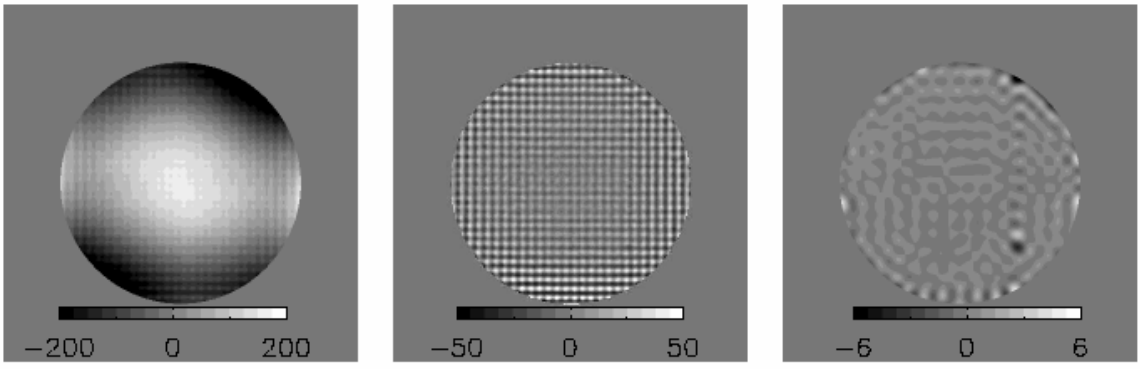

Figure 9. Wavefront measurements of 1024 element in a high-contrast imaging testbed showing the initial wavefront before applying the closed-loop control (right), after flattening the wavefront (center), and after applying the high-frequency spatial filter to remove errors outside of the controllable regime (left).

An interferometric measurement of a 1.9x2.5mm subaperture (figure 10) shows an unpowered surface quality of 12.4nm RMS the 1024 MEMS DM. Also visible in this measurement are the periodic surface features resulting from small mirror attachment posts and print-through from underlying structures.

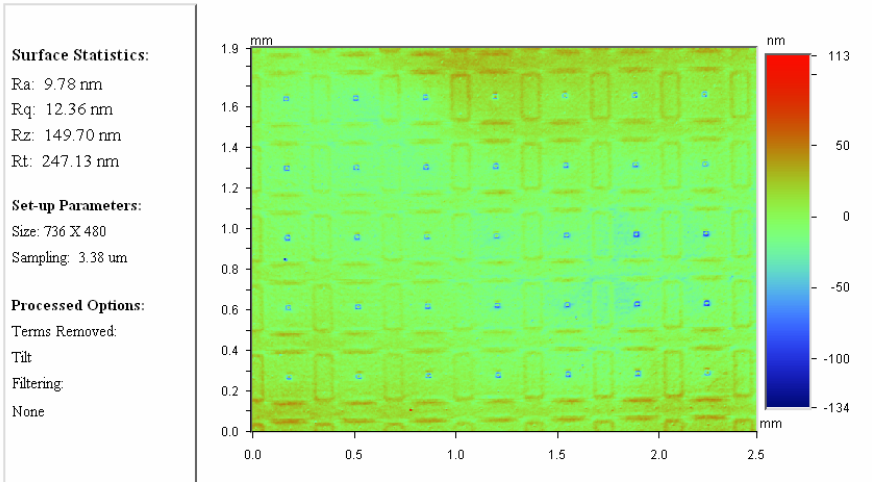

Figure 10. Interferometric surface measurement of 5x7 actuator region of the 1024 element MEMS DM showing am unpowered surface roughness of 12.4nm RMS.

The PICTURE program, led by a team at Boston University collaborating with MIT and NASA's Jet Propulsion Laboratory, will mark the first use of a MEMS deformable mirror in a space-based astronomical observation platform. The launch of the PICTURE mission is scheduled for April of 2007.

4. 4096 ELEMENT CONTINUOUS FACESHEET MEMS DM FOR GEMINI PLANET IMAGER (GPI)

A 4096 element, continuous facesheet MEMS deformable mirror is currently under development for the Gemini Planet Imager (GPI) instrument. In an experimental "Extreme Adaptive Optics" testbed a 1024 element MEMS deformable mirror was characterized to determine if the technology is suitable for this application. The testbed showed that the MEMS DM could be flattened to less than 1nm RMS within controllable spatial frequencies over an aperture of 9.2mm with an average long term stability of less than 0.18nm RMS phase [6], thereby demonstrating that the MEMS DM is a feasible wavefront compensator for high contrast imaging. A 4096 element MEMS DM with a stroke of up to 4µm, and a surface figure of 10nm RMS is required for the GPI instrument. Although MEMS DMs with array sizes up to 32x32, and 4µm stroke, and 10nm RMS surface quality have been demonstrated they have not all been achieved on the same device.

Table 2 lists the device requirement to enable high-contrast imaging in the Gemini Planet Imager. Although some of these parameter have been achieved on existing Boston Micromachines MEMS DMs, they have not all been achieved simultaneously on a single device.

Table 2. 4096 Element MEMS Deformable Mirror Requirements

Description	Requirement
Pixel count	4096 (64x64 array)
Square Pitch	300 to 400 µm
Stroke	2-3 µm, after mirror is fully flattened to within 70 (RMS)
Fill Factor	99%
Active Aperture size	19.2 mm (48 actuator diameter @ 400µm pitch)
Pixel surface finish (RMS)	<10 nm
Pixel surface finish (P-V)	3 times "Pixel surface finish (RMS)"
Flatness over aperture	<70 nm (tilt & sphere removed) (RMS)
Bandwidth	~2.5 kHz
Inter-Actuator Stroke	1µm
Yield	100% of actuators on a 48 actuator diameter circular aperture function to spec.
Operating Temperature	-30C

Achieving the stroke, bandwidth, and surface finish requirements for the 4096 element deformable mirror require careful design considerations for the actuator design since each of these performance parameters affect the others. Increasing stroke requires a decrease in actuator stiffness for a given voltage, which therefore reduces the overall bandwidth of the DM and also affects the overall figure of the mirror facesheet resulting from the fabrication process used to manufacture the MEMS DMs. To achieve the desired stroke of 2-3µm after the mirror is fully flattened, a 4µm stroke actuator design on a 400µm pitch, was chosen, providing sufficient stroke in the DM to meet this goal and allowing the device to operate with sufficient margin over its critical deflection. As shown in Figure 11, over 4µm of stroke has been achieved with the first devices fabricated in this initial phase of this development effort. The electromechanical behavior of these devices is shown in figure 12. Over 4µm of stroke is achieved using different actuator designs, at operating voltages between 210 and 280V. The trade-off between these MEMS DM designs is pixel surface figure, natural frequency, and the maximum operating voltage. The measured surface figure over a 1x1mm area of the device designs reported on in figure 11 is 18.6, 9.2, and 6.4nm RMS respectively (tilt & curvature removed).

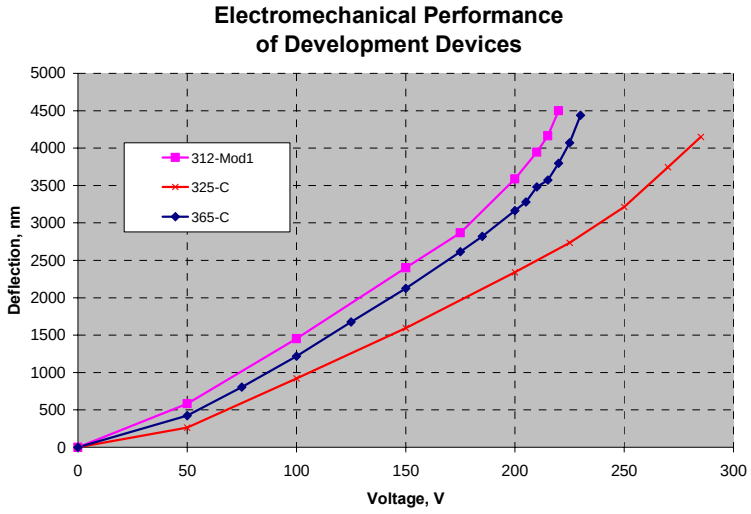

Figure 11. Deformable mirror deflection as a function of voltage applied to an array of 3x3 actuators. Over 4 µm *of stroke is achieved on these development devices at operating voltages between 210 and 280V.*

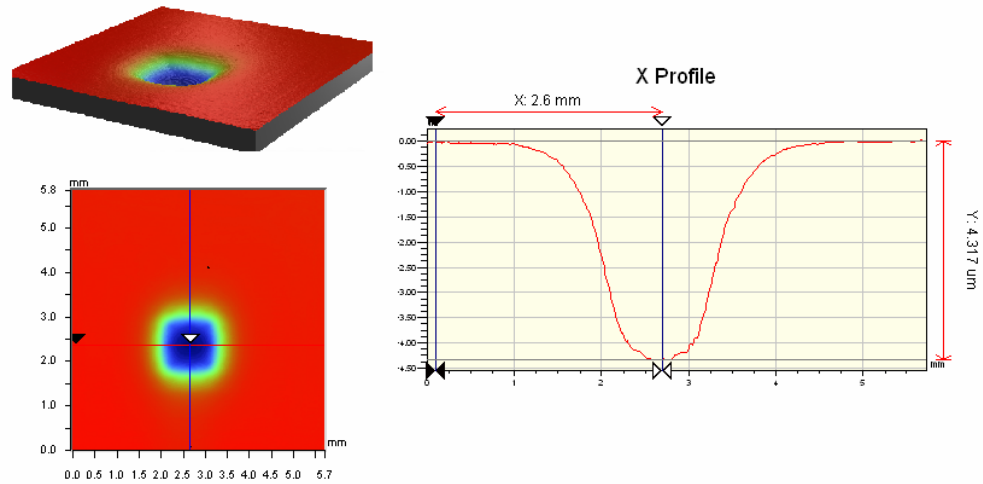

Figure 12. Measurement of 144 element MEMS DM in which a 3x3 array is pulled down to over 4µm of deflection

The inter-actuator stroke of this device was measured by moving the entire DM facesheet down to its halfway deflection point (~2um) after which one actuator was pulled down to the maximum operating voltage while the voltage on its nearest neighbor was released such that a push/pull effect was generated. As shown in the surface measurement if Figure 13, an inter-actuator stroke of over 1.1um was achieved.

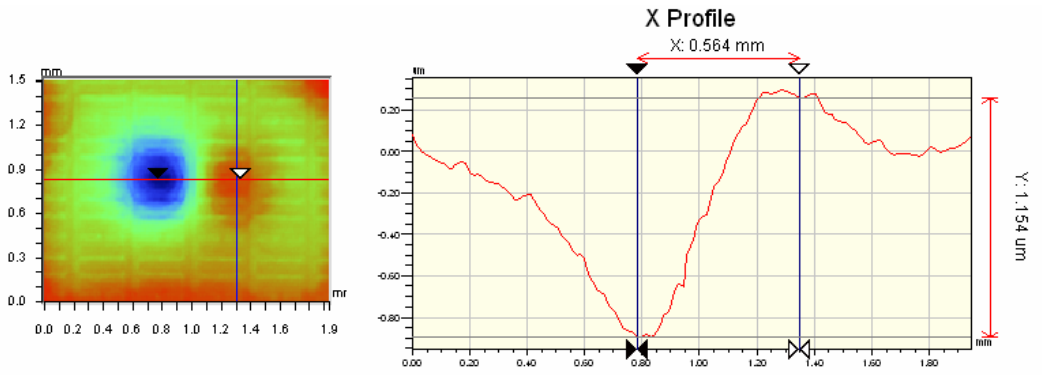

Figure 13. The inter-actuator stroke between two neighboring elements on the baseline MEMS deformable mirror design was measured to be 1.15µm.

A prototype 4096 device was also fabricated to investigate the effects of the large DM on the fabrication process. Actuators were coupled together in groups of various sizes to get an indication of actuator yield on a single device. The device revealed a high yield on actuator functionality (of 1500 actuators tested, 100% were responsive). A Zygo interferometer was used to characterize the surface of the device, shown in figure 14. The continuous facesheet mirror on this device has a low-order spherical term with a peak to valley of ~600nm resulting from various chemomechanical polishing steps in the fabrication process. Although this may be corrected for by a low-order "woofer" DM in the GPI instrument, corrective actions for these surface effects are being investigated to reduce these surface effects.

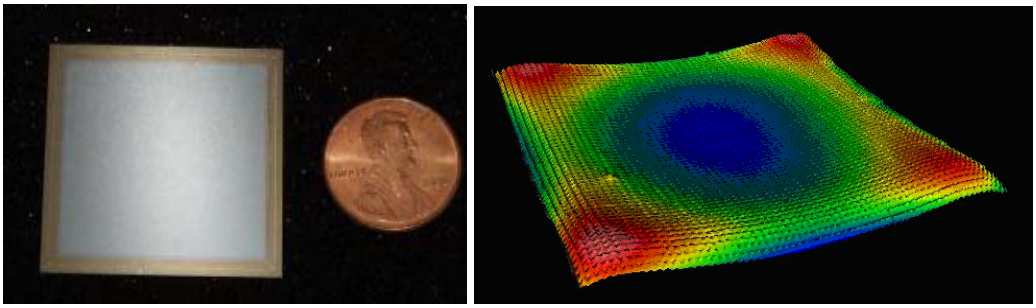

Figure 14. A Prototype of 4096 element MEMS deformable mirror -68x68 array with central 64x64 array active (left). A measurement of the overall surface figure of this device shows a P-V surface variation of ~600nm (right).

5. 331 ELEMENT TIP-TILT-PISTON MEMS DM FOR VISIBLE NULLING CORONOGRAPH

The new MEMS DM, shown, in figure 15, is being developed for the visible nulling coronagraph instrument for NASA's Terrestrial Planet Finding mission (TPF-c) seeking to optically detect, characterize and study Earth-like extrasolar planets located in the habitable zones of nearby stars. To achieve the required contrast ratio of 10^9 to meet this objective, the coronagraph optical system requires a unique DM design that performs conventional wavefront correction, but also has a tip/tilt feature to control sub-aperture coupling to the fiber optic spatial filter [8,9]. For the nulling coronagraph it is essential to have 0.1nm piston, and 0.06 arc-seconds tip/tilt resolution, nanometer level stability, and ultra-flat (<10nm RMS) mirror segments.

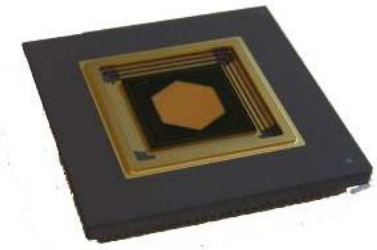

Figure 15. TPF-C MEMS, 331-element, tip/tilt/piston DM

The TPF MEMS DM is based largely upon existing MEMS DM technology used for the continuous facesheet DMs although the design and fabrication processes are tailored to the requirements of the visible nulling coronagraph. Figure 16 shows an illustration of the TPF DM architecture. The DM will have an active aperture of 9.5mm and consist of a hexagonal array of 331 mirror segments each of which is supported by three double cantilever electrostatic actuators, similar to those used in the previously described devices.

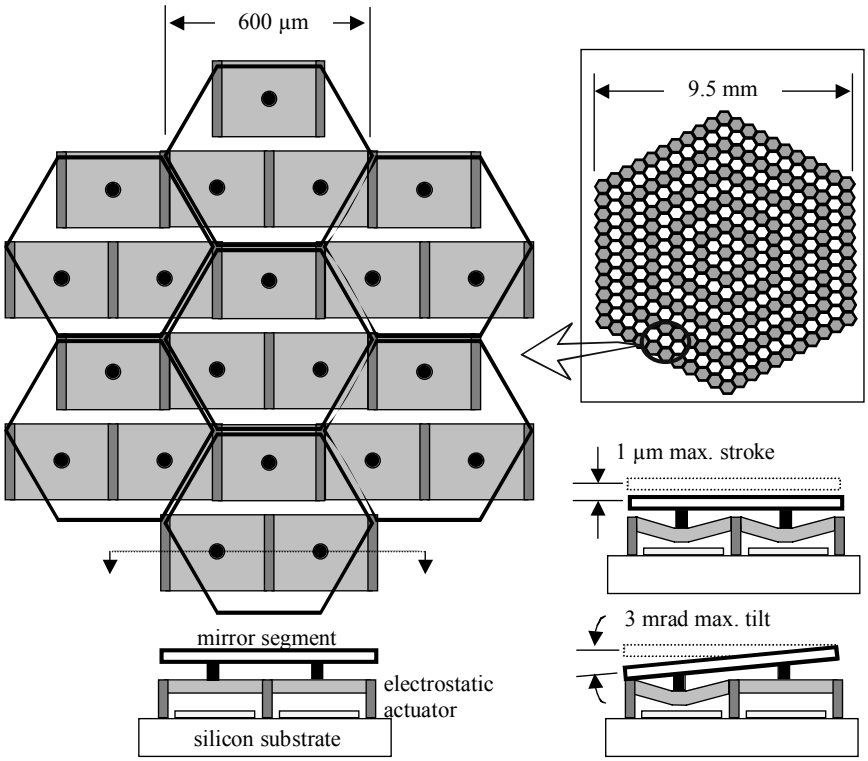

Figure 16. Schematic of the TPF MEMS DM. 331 hexagonal mirror segments (top right) are arranged in a close-packed array, with 2µm spacing between segments to yield a fill factor of 99.2%. Each segment in the array will be supported by three posts (top left) attached to an underlying array of double-cantilever electrostatic actuators. A cross section through one pair of actuators (bottom left), illustrates the basic parallel-plate design. Common or differential deflection of actuators will yield piston or tilt motions or the mirror segment, respectively (bottom right.) By controlling the voltage applied to each of these three actuators 1µm of stroke and 3mrad of tilt can be achieved simultaneously.

To minimize bending of the mirror segment during tilt motions, due to mechanical moments induced on the mirror through the actuator attachment posts, a gimbal flexure is integrated with the double cantilever actuator. Performance testing on these devices has demonstrated the effectiveness of these flexures. The measurements shown in figure 17, demonstrate that on a device with a 3µm thick mirror segment the change in surface flatness due to the bending is reduced from more than 15nm RMS to less than 5nm RMS at a tilt angle of 3mrad. By utilizing these flexures and increasing the thickness of the mirror segment to ~10µm to stiffen the segment, this flatness change will be reduced to less than 1nm RMS.

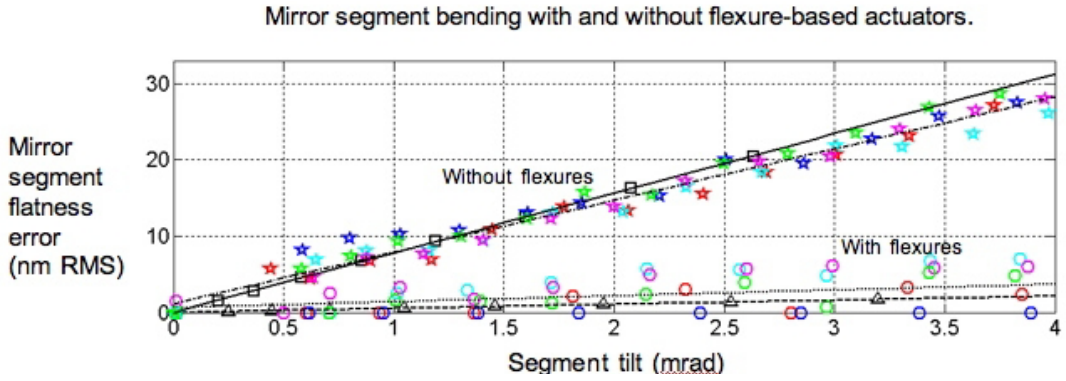

Figure 17. Measurements of TPF device with a 3µm thick mirror element showing the change of mirror segment flatness due to bending as a function tilt angle. Mirror segment flatness becomes greater than 15nm RMS at 3mrad of tilt for devices not utilizing the flexure compared to less than 5nm for those using the flexure actuator design.

To achieve the flat-mirror pixel a new fabrication process has been developed that uses a thick layer of epitaxially-grown polysilicon allowing the mirror surface to be polished to a smoothness of ~1nm RMS and eliminating most of the print-through effects that are present on the surface quality of the continuous facesheet devices. Controlling the stress in these films is critical to achieving the desired flatness since the stress gradient through the thickness of the film will cause it to curve. As shown in the measurement in figure 18, by controlling the film deposition parameters and introducing multiple anneal steps mirror segments with an overall flatness of 2.8nm RMS, (1nm RMS in a 250µm diameter subaperture) have been fabricated.

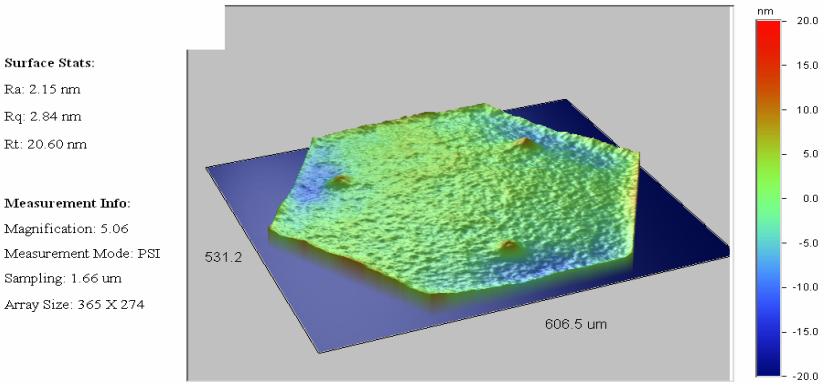

Figure 18. Measurement of hexagonal mirror element after anneal showing a surface flatness of 2.8nm RMS over the entire surface.

6. CONCLUSION

Three different MEMS deformable mirrors for adaptive optics in astronomical observation have been presented. Each of these devices will be used for extrasolar planet detection in their respective instruments and the performance of the MEMS DMs are to meet the specific needs of the mission. The scalable architecture of the MEMS deformable mirrors presented here have the advantage of compactness, high actuator counts, and low cost, due to the batch fabrication processes used to manufacture them, which make them well suited for ground-based observation platforms correction and where many DMs may be used in multi-object AO, multi-conjugate AO instrument. For space-based applications in particular, the low-power consumption and light-weight inherent in these electrostatically actuated devices present a major advantage over macroscale deformable mirrors.

7. REFERENCES

1. M.C. Roggemann, B.M. Welsh, R. Q. Fugate, "Improving the Resolution of Ground based telescopes", Reviews of Modern Physics, Vol. 69, No.2, April 1997.
2. Macintosh, B., Graham, J., Oppenheimer, B., Poyneer, L., Sivaramakrishnan, A., Veran, J., "MEMS-Based Extreme Adaptive Optics for Planet Detection"**,** Proc. SPIE Vol. 6113, 611308 (Jan. 23, 2006)
3. Marc J. Kuchner, David N. Spergel,, "Terrestrial Planet Finding with a Visible Light Coronagraph", Scientific Frontiers in Research on Extrasolar Planets, ASP Conference Series, Vol. 294, D. Deming and S. Seager, eds., 2003
4. Perreault, J. A., Bifano, T. G., Levine, B.M., and Horentein, M., "Adaptive optic correction using microelectromechanical deformable mirrors," Opt. Eng. [41]5, pp. 561-566, 2002
5. Bifano, T., Perreault, J., Mali, R., et al., "Microelectromechanical deformable mirrors", IEEE J. of Selected Topics in Quantum Electronics, 5 (1): 83-89 Jan-Feb 1999.
6. Evans, J., Morzinski, K., Severson, S., Poyneer, L. Macintosh, B., Dillon, D., Reza, L., Gavel, D., Palmer, D., Olivier, S., and Bierden, P, "Extreme adaptive optics testbed: performance and characterization of a 1024-MEMS deformable mirror"**,** Proc. SPIE Vol. 6113, 61130I (Jan. 23, 2006)
7. F. Miyahira, H. D. Becker, "Total Dose Degradation of Optical MEMS Mirrors", T*IEEE Nuclear and Space Radiation Effects Conference (NSREC)*, Monterey, California July 21-25, 2003
8. B. M. Levine, M. Shao, D. Liu, J. K. Wallace, and B. Lane, "Planet detection in visible light with a single aperture telescope and nulling coronagraph" Proc. SPIE, **5170** (2003).
9. M. Shao, E. Serabyn, B. M. Levine, B. Mennesson, and T. Velusamy, "Visible nulling coronagraph for detecting planets around nearby stars" Proc. SPIE, **4860** (2002).